

DETC2012-70634

DESIGN, DEVELOPMENT AND PRELIMINARY ASSESSMENT OF GRASPING DEVICES FOR ROBOTIZED MEDICAL APPLICATIONS

Olivier Piccin, Nitish Kumar, Laurence Meylheuc, Laurent Barbé, Bernard Bayle
LSIIT (UMR CNRS–UdS 7005)
INSA Strasbourg
University of Strasbourg
Email: olivier.piccin@insa-strasbourg.fr

ABSTRACT

This paper presents the development of NGDs (needle grasping devices) capable of handling elongated objects such as surgical needles. After describing the main demands of medical needle-based procedures, a requirement list for a typical NGD is presented. Some solution principles for a grasping device are generated, combined and then classified to obtain a set of principle variant solutions. The design study of some of these variant solutions is then developed and a discussion on two device candidates constructed using either interconnected rigid bodies or compliant parts will be presented. The mechanical behavior of the compliant mechanism acting on a needle barrel is simulated with a FEM analysis including the model of non-linearities induced by large deformations and the contact between the needle and the grasping device. Functional prototypes of both NGDs have been constructed and a first experimental assessment of their service capability is finally exposed.

1 INTRODUCTION

Grasping and manipulation of surgical needles represent a very common concern in many medical specialties involving image guided needle insertions. This paper presents the development of two grasping devices capable of handling such elongated objects. More specifically, the principal motivation of the proposed work originates from the need to insert needles in the context of interventional radi-

ology. In this medical specialty, minimally invasive procedures are performed to diagnose or treat pathologies under image guidance. The medical interventions targeted by the devices presented in this paper encompass the wide class of procedures that necessitate needle insertion such as biopsies, radiofrequency ablations or cancer local delivery treatments.

Among the various imaging modalities available, computed tomography (CT) and fluoroscopy provide a fast and accurate visual feedback to the radiologist and are now very widely used in medical routine. However, repeated CT and fluoroscopy endanger physicians with potentially harmful ionizing radiations. That is the main motivation for developing teleoperated robotic assistant to remotely insert needles under CT guidance.

A possible layout of teleoperated percutaneous procedures was presented in [1]. It is composed of a master station protected from the radiation source and operated by the physician using a haptic interface. At the remote site, the slave station comprises the CT scanner, the patient and the robotic assistant dedicated to the percutaneous procedure. This layout enables the radioprotection of the medical staff but also provides the practitioner with a haptic feedback on the insertion task which is highly desirable for safety reasons.

In this paper, the specific need of grasping an elongated object such as a needle is focused upon. The corresponding needle grasping device (NGD) is mounted as a tool on the

robotic assistant as indicated in Figure 1.

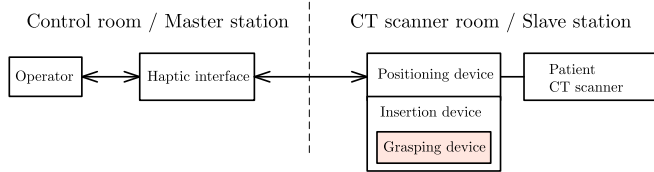


FIGURE 1. THE NEEDLE GRASPING DEVICE WITHIN THE GENERAL LAYOUT OF TELEOPERATED PERCUTANEOUS PROCEDURES.

2 REQUIREMENTS STEMMING FROM THE TARGETED APPLICATION

Now the specific conditions that the grasping device has to meet, is detailed. The available space between a CT-scan ring and a patient is often a limiting factor. Depending on the patient's build, the free volume for the robotic assistant is at most of the order of 200 mm^3 . As this volume is just a slightly higher than the length of most biopsy needles, the grasping device size should be as small as possible.

In addition, it would be beneficial to comply with existing surgical needles, in terms of diameter and length, and thus avoid the use of device specific needles.

Another important feature for the NGD is the capacity to allow a wide aperture around the needle when opened as well as to get the needle centered during re-grasping of the needle. This demand originates from the fact that the needle insertion is not a one step task. Indeed to avoid internal tissue laceration and improve gesture accuracy, the insertion motion itself is generally done during a short patient's apnea. After that, the non-inserted part of the needle requires to be released to comply with the motion exerted by the internal perforated organs. At this stage the needle should move freely off a central position about the entry point on the patient's skin. To perform the following insertion step the grasping device should be capable to re-center and re-grasp the needle.

One optional but very desirable feature of the grasping device corresponds to the possibility of rotating the needle about its axis. This capability is useful to rotate the needle bevel and to provide some possibilities to avoid anatomic obstacles such as bones or to facilitate the needle steering. On the side of force transmission, the grasping device should sustain a maximum insertion action of 15N and allow haptic feedback, more precisely, be compatible with real-time insertion force measurement. To avoid needle deterioration the grasping device should ideally incorporate a grip

limiting scheme. Concerning the material requirement, the grasping device should not generate artefacts in CT scanner images so its construction needs to set a good level of radiolucency. And the concluding items in this requirement list are the safety and sterilization properties pertaining to the medical context.

TABLE 1. REQUIREMENT LIST FOR A NEEDLE GRASPING DEVICE.

<ol style="list-style-type: none"> 1. Geometry <ol style="list-style-type: none"> a - Minimal volume 2. Kinematics <ol style="list-style-type: none"> a - Allow grasping of different size needles: 0.5-2.4mm in diameter b - Allow a wide aperture around the needle c - Needle centering d - Self rotation about the needle axis 3. Forces <ol style="list-style-type: none"> a - Sustain a maximum insertion force of 15N b - Limitation of the grasping force c - Compatible with insertion force measurement 4. Material <ol style="list-style-type: none"> a - Radiolucency
--

From literature survey several systems dedicated to needle insertion that consequently provide solutions for needle handling, could be identified. The most frequent working principle involves opposing rollers to perform simultaneously the needle grasping as well as its insertion motion (e.g. Refs [2, 3]). However, axial insertion force measurement turns out to be very difficult or even impossible with this principle since the force measurement highly depends on the friction conditions with the needle barrel. To add this important functionality of axial insertion force measurement to a needle insertion device, it seems necessary to uncouple the needle displacement from its grasping.

For instance, the axial force measurement issue is addressed in the system developed by Badaan *et al.* [4] with an off-the-shelf sensor set on the transmission chain of the insertion motion. In this system, the grippers are snapped manually on the needle before the insertion starts and can be reopened on-demand to release the needle. However, it does not provide a controlled feature for recentering and gripping back the needle during insertion.

During the initial development of this work, the need to release and regrasp the needle during the insertion procedure has been overlooked and thus the kinematic requirement 2.b was missing in the early first miniature-chuck-

based device presented in [5]. This functionality was included in the chuck described in [1].

Finally, the Table 1 summarizes the list of the identified requirements for a NGD.

3 NEEDLE GRASPING DEVICE DESIGN

3.1 Problem Statement and Solution Principles

To establish the functional structure of a NGD, mainly four elementary subfunctions are considered, which can be formulated as (1) put obstacles around the needle, (2) move obstacles radially, (3) transmit motion to the obstacles and (4) actuate moving obstacles.

This decomposition tends to formulate the essential problems at a higher level of abstraction in order to leave open possible solutions and make a systematic approach easier [6]. The Table 2 presents several solution principles for the NGD subfunctions.

In the first row, the columns 1 to 5 describe several design principles to fulfill the subfunction SF₁. The simplest embodiment for this subfunction requires at least two opposing obstacles acting radially on the needle as described in the sketches 1 to 3. The solutions 4 and 5 suggest a higher number of obstacles in operation for gripping the needle barrel. Another important design option refers to how obstacles move with respect to the needle and how many contact points each obstacle does have with the needle.

TABLE 2. SOLUTION PRINCIPLES FOR THE SUBFUNCTIONS OF A NGD.

		Solution Principles				
		1	2	3	4	5
Subfunctions	1 SF ₁					
	2 SF ₂					
	3 SF ₃					
	4 SF ₄					

In the second row of the table are presented some options to realize the motion of the obstacles. Basic ideas

depicted in the first two columns correspond to a simple pivoting or translation of the obstacle. The solution principle 3 moves the obstacle using a radial slider driven by a slot-follower element. Columns 4 and 5 present two possible planar and spatial linkages that could serve for the obstacle motion. At this stage, the required motion to impart to the obstacles could be a rotation or a translation. Therefore, the last two rows of the table describe possible choices for actuation and transmission of the required motion to the obstacles.

In light of the proposed classification scheme, the gripping device of the Robopsy system [3] corresponds to the solution variant of the first column, namely 1.1–2.1–3.1–4.1 whereas the two grasping devices developed in prior research [1, 5] can be related to the variants 1.4–2.3–3.1–4.1 and 1.3–2.3–3.2–4.1. In the section 3.2, construction details of the rigid-body NGD first presented in [1] will be given.

The two most promising design candidates have been selected based on the existing chuck (variant 1.3–2.3–3.2–4.1) for the first one and based on a new solution variant 1.5–2.5–3.2–4.1 for the second. The first one uses interconnected rigid bodies whereas the second employs some compliant parts. Following sections detail the design and the construction issues relative to these two NGD variants.

3.2 Rigid-Body NGD

Existing NGD presented in [1] is used as a starting point to detail its construction issues. The proposed chuck comprises of a main body, two jaws, two pairs of rods and a gear as described in Figure 2. During the tightening of the chuck, the displacement of each jaw is a translation along the direction followed by the rods 1 and 2 inside the slots 1 and 2 on the main body. Simultaneously, each chuck is driven by the slots 3 constructed within the bore of the gear and followed by the rods 1 (which are longer than the rods 2) when the gear is rotated about its axis.

The central problem for designing this type of NGD consists in constructing adequate slots on the gear to obtain the desired grasping function. The construction of the slots 3 within the gear must be compatible with the translation of the jaws within the main body. This problem can be reformulated geometrically using a kinematic inversion for the chuck mechanism. The gear is now considered as fixed to the ground and a jaw is moving with a combined motion of translation and rotation. During this displacement, the line Δ coincident with the axis of the rod 1 intersects the cylinder C formed by the bore of the gear and the resulting curves can be used to cut the appropriate slots 3 in the gear. To this end, it is required to determine the equations of these curves.

Let us denote $\mathcal{F} = (O, \mathbf{x}, \mathbf{y}, \mathbf{z})$ a reference frame, such

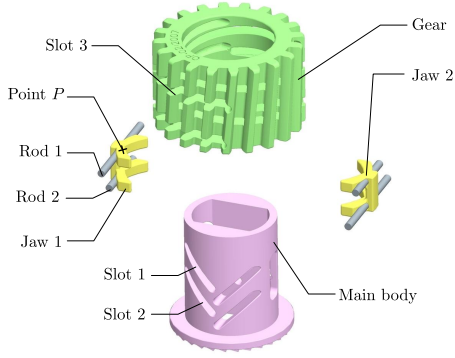


FIGURE 2. EXPLODED CAD VIEW OF A RIGID-BODY NGD [1].

that the cylinder \mathcal{C} has (O, \mathbf{z}) as its axis and radius R .

The line Δ is undergoing a combined motion of rotation and translation in space and its intersecting curves with the cylinder \mathcal{C} need to be determined. Additionally, the line Δ always lies in a moving plane which keeps orthogonal to the cylinder axis.

The line Δ is defined by a point P and a unit vector \mathbf{u} and an orthonormal basis $(\mathbf{u}, \mathbf{z}, \mathbf{n})$ is attached to Δ . The configuration of Δ with respect to \mathcal{F} can be described using three parameters $\theta = (\mathbf{x}, \mathbf{n})$, $r = \mathbf{OP} \cdot \mathbf{n}$, $z = \mathbf{OP} \cdot \mathbf{z}$ as indicated in Figure 3.

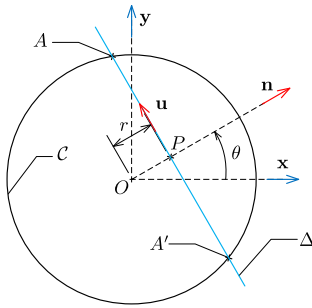


FIGURE 3. PARAMETERIZATION OF THE MOVING LINE Δ .

Depending on the value of r with respect to R , there may be no solution ($r > R$), one single point solution when $r = R$ or two solution points (A and A') when $r < R$. This last case is studied, since the other ones are of no practical interest. In this case, the moving line Δ generates two spatial curves Γ and Γ' traced on \mathcal{C} corresponding to the set of points A and A' . It should be noted that each of two points A and A' are symmetric with respect to the axis (O, \mathbf{n}) .

The intersection curves Γ and Γ' can be described by the vector function

$$\mathbf{\Gamma}_\varepsilon(\theta, r, z) = r \mathbf{n} + \varepsilon \sqrt{R^2 - r^2} \mathbf{u} + z \mathbf{z} \quad (1)$$

where r , θ and z are functions of a parameter t chosen in the interval $[0; 1]$ and where the value ε , taken in set $\{-1; +1\}$, determines the curve Γ or Γ' . For sake of simplicity the functions were chosen linear with respect to t as following:

$$\begin{cases} r(t) = r_{max}t & (2) \\ \theta(t) = \theta_{max}t & (3) \\ z(t) = z_{max}t & (4) \end{cases}$$

where r_{max} , θ_{max} and z_{max} denote constant parameters describing the final position of Δ . Figure 4 depicts the intersection curves Γ and Γ' , defining the geometry of the slots 3 drawn for some values of the rotation angle θ_{max} .

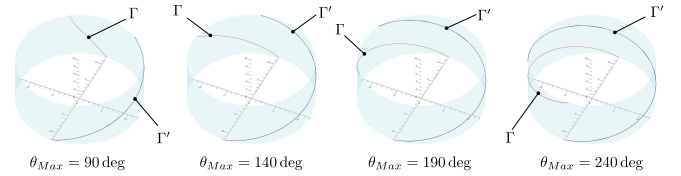


FIGURE 4. INTERSECTION CURVES Γ AND Γ' FOR SOME VALUES OF θ_{max} .

To fulfill a slot-follower function for each jaw it is necessary to generate two couples of curves Γ and Γ' with sufficient axial offset along the cylinder axis to ensure a minimum wall thickness between the slots and to avoid any curve crossing. The influential parameter to validate this condition is the angle of rotation θ_{max} which was set to 140 deg.

The resulting NGD can provide a theoretical grasping force F exerted by each opposing jaw on the needle barrel which is related to the driving torque τ_m applied by the motor

$$F = \frac{n\theta_{max}}{n_j r_{max}} \tau_m \quad (5)$$

where n and n_j denote respectively the number of teeth of the gear and the number of jaws (here, $n_j = 2$).

3.3 Flexible-Body NGD

The second design candidate that is considered here uses thermoplastic flexible parts. In this design variant the number of moving obstacles is increased to three. Constituting parts of this NGD are shown in Figure 5 and include a main body on which, three flexible jaws equipped with high grip neoprene pads, are hinged. Each jaw is then connected to the gear via a pin joint. Simultaneously, the gear is guided in rotation with respect to the main body part.

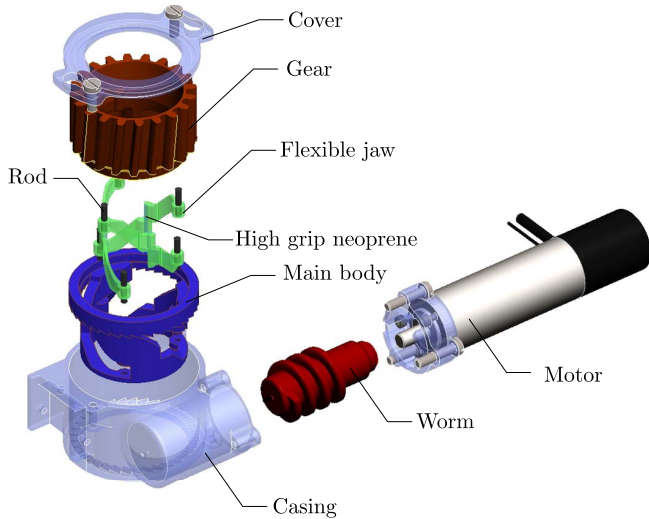


FIGURE 5. EXPLODED CAD VIEW OF THE FLEXIBLE NGD WITH THE SERVO ACTUATOR.

The implementation of this design candidate requires the use of spatial arrangement of the joints at the end of each jaw. The geometry of the jaw has been iterated to provided two interrelated models, namely a pseudo-rigid-body model [7] and the corresponding flexible and monolithic form of the model as described in Figure 6.

3.3.1 Pseudo-Rigid-Body Modeling To investigate the NGD behavior and iterate its design, a pseudo-rigid-body model has been constructed in which each jaw was segmented into three rigid links connected by pin joints as indicated in Figure 6(a). During the NGD operation, the end point A_1 of a flexible jaw is hinged to the fixed main body part whereas the other end point B_1 is driven on a circle by the rotating gear as depicted in Figure 7. The NGD closes with a 90 deg rotation of the gear and allows a maximum clearance included within a cylinder with diameter 24 mm. The theoretical grasping force of each jaw can be calculated using equation (5) with $\theta_{max} = 90$ deg,

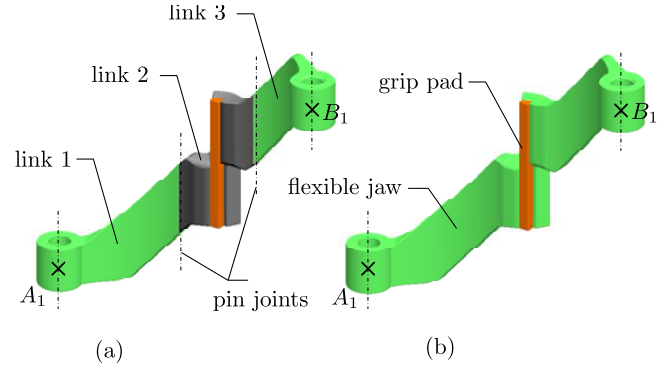


FIGURE 6. CAD VIEW OF ONE FLEXIBLE JAW IN PSEUDO-RIGID-BODY FORM (a) AND IN MONOLITHIC FORM (b).

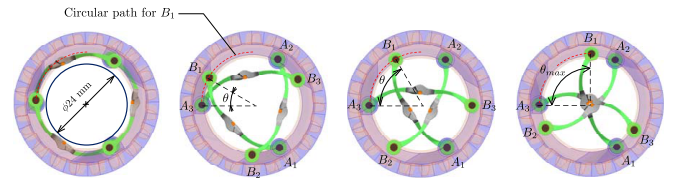


FIGURE 7. CAD TOPVIEW OF THE FLEXIBLE NGD OPERATION.

$$r_{max} = 12 \text{ mm and } n_j = 3.$$

3.3.2 Flexible-Body Modeling When considering the jaws as deformable bodies, the closing of the NGD causes a coordinated motion and deflection of the three jaws around the needle. In the case of thermoplastic parts such as those considered in this NGD, the low material stiffness and yield strength could create the conditions for nonlinear behaviors to occur [8]. However, in the proposed NGD design, the dominant source of non-linearities comes from geometry and the occurrence of contact conditions between the jaws and the needle. Thus, it is assumed here that the problem includes mainly geometric and contact nonlinearities and can be consistently solved using linear material behavior. As a result, the large displacement imposed to the jaws generates stresses and strains on the deformable parts which need to be calculated to check both the NGD's functionality and the parts failure. For this purpose, two operating phases for the modeling of the flexible NGD are considered which are following : i) the motion of the jaws in free space during the NGD closing and ii) the interaction with the needle barrel during the grasping itself. This loading scenario requires the modeling of large strains induced by the large displacement of the jaws rotated by the gear.

This problem has been solved with a nonlinear FEA code allowing contact analysis.

Meshing The geometry of the parts were imported from CAD and included a segment of the needle and the three jaws equipped with high grip pads. The resulting mesh shown in Figure 8 (a) uses 4-node tetrahedral elements for the jaws and the neoprene pads and 6-node wedge elements for the needle. Meshing of the jaws and the pads has been refined in regions where large stress gradients are expected such as in the contact area. The total number of nodes for the entire model is 36 270. Each part of the FEA model was assigned with the corresponding material namely polymer resin for the jaws (PX220, Axson Tech. Inc.), neoprene for the pads and stainless steel for the needle. The polymer resin was chosen to be compatible with the fabrication process described in subsection 3.3.3.

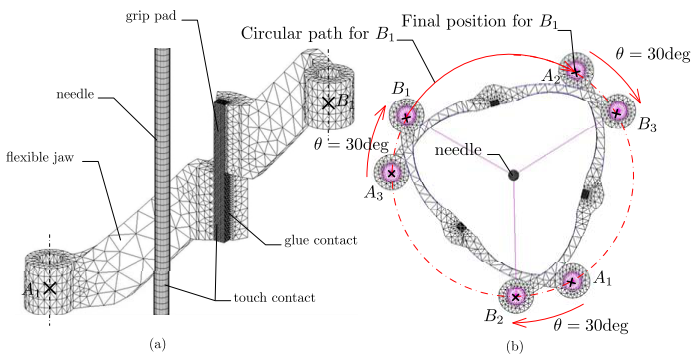


FIGURE 8. MESH FOR ONE OF THE FLEXIBLE JAW AND A PORTION OF THE NEEDLE (a), BOUNDARY CONDITIONS AND LOADS APPLIED ON THE FLEXIBLE NGD (b).

Boundary and loading conditions The modeling of the pin joints at both ends of each jaw is conducted using rigid body elements. A node at the hole center is rigidly connected to all the nodes on the hole circumference as indicated in Figure 8 (b). This technique blocks the node motion in the radial direction but leaves them free to rotate about the hole center. The points A_i and B_i ($i = 1..3$) are respectively attached to the fixed main body part and the rotating gear. Contacts are set between the jaws and the grip pads (indicated as glue contacts in Figure 8 (a)) whereas contact areas between the grip pads and the needle barrel are specified in the model and denoted touch contact in Figure 8 (a).

Loading conditions on the jaws are applied in the form of imposed displacements of the points B_i along a circular path centered with the needle axis.

Results The resolution of the problem with three moving jaws has been solved. firstly the displacements of the jaws during the closing of the NGD was understood. Figures 9 (a) and (b) present the displacements of the deformed shapes of the NGD with an indication of the starting configuration plotted in wireframe display style. As the first contact between the grip pads and the needle is gained at the configuration $\theta = 88\text{deg}$, the analysis has been continued until $\theta = 120\text{deg}$.

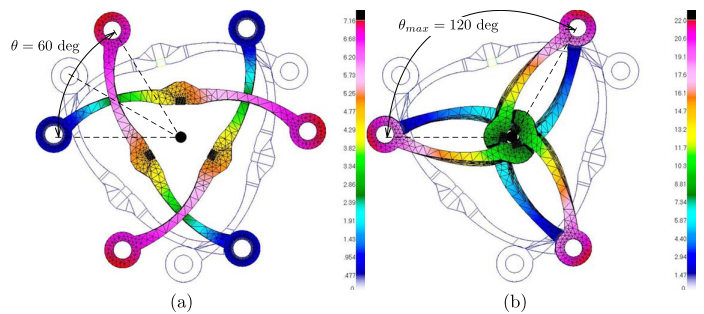


FIGURE 9. DISPLACEMENTS DISTRIBUTION FOR THE FLEXIBLE NGD AT INTERMEDIATE POSITION $\theta = 60\text{deg}$ (a) AND AT FINAL POSITION $\theta_{max} = 120\text{deg}$ (b).

At this fully tighten position, the principal maximum strain for the jaw is located in the central area of the part as shown in Figures 10 (a) and (b). Its value is in the order of 10 % which corresponds to the elongation at break for the chosen resin.

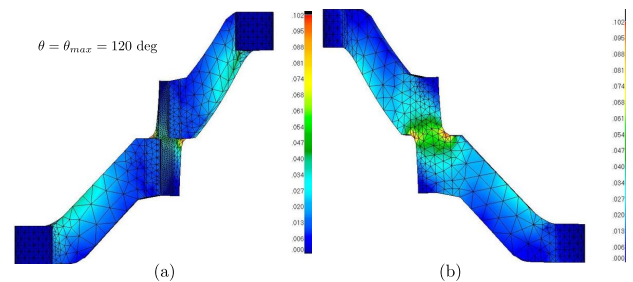


FIGURE 10. PRINCIPAL MAXIMUM STRAIN FOR THE FLEXIBLE NGD AT THE FULLY TIGHTEN POSITION $\theta = 120\text{deg}$: FRONT VIEW (a), BACK VIEW (b).

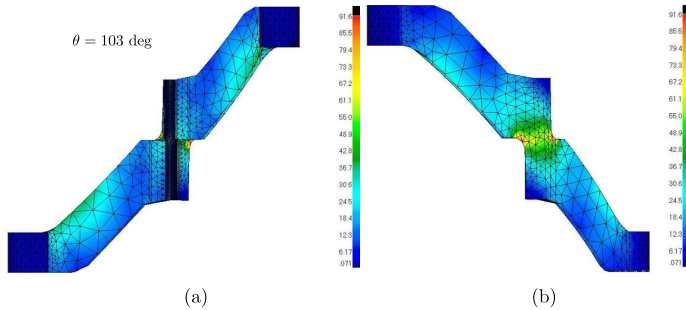


FIGURE 11. VON MISES STRESSES CALCULATED FOR THE FLEXIBLE NGD AT THE ANGULAR POSITION $\theta = 103$ deg: FRONT VIEW (a), BACK VIEW (b).

The Von Mises stresses in the configuration $\theta = 103$ deg are displayed in Figures 11 (a) and (b) for a single jaw. The maximum VM stresses are also located in the central area of the part as shown in Figure 10 (b). The location of stress concentration coincide with the highest level of strain. After reviewing the Von Mises stress results, one can note that the the yield stress is reached for $\theta = 103$ deg. Consequently, a rotation of the gear by an angle in the range 103-120 deg may potentially deforms the jaws irreversibly.

3.3.3 Fabricated Prototype The flexible NGD has been fabricated using rapid prototyping techniques. The most critical parts in the NGD are the jaws due to the high level of strain and displacement applied on them. Consequently, the required mechanical properties for the jaws turned out to be difficult to obtain with classical 3D printing machines. Starting from a master part corresponding to the jaw fabricated with a conventional 3D printing machine, a silicon mold was constructed and a small series of parts could then be obtained using vacuum casting.

4 EXPERIMENTAL ASSESSMENT

Most important functional characteristics of the proposed NGDs is their ability to maintain the grip on the needle, over the range of forces and range of rate of change of forces applied to it. Objective of the experiments is to characterize the grasping capability of the both proposed NGDs and assess the maximum force sustained by the NGDs, without allowing the needle to slip. In real medical applications, rate of change of force may vary depending upon the density of tissues encountered. For example, at the rupture of tissues there are sudden changes in force over very small periods of time.

4.1 Experimental Setup

Experimental setup consists of a traction machine from Zwick, GmbH (Z005 THN - Allround Line), capable of applying varying magnitudes of force and rates of change of force to the cross-head. A 18 gauge (1.3 mm), polished, stainless steel needle is held between the jaws which is attached to the cross-head. Both NGDs are actuated by a Harmonic Drive DC servo motor (RH-5A-5502) which is controlled by another computer via I/O cards.

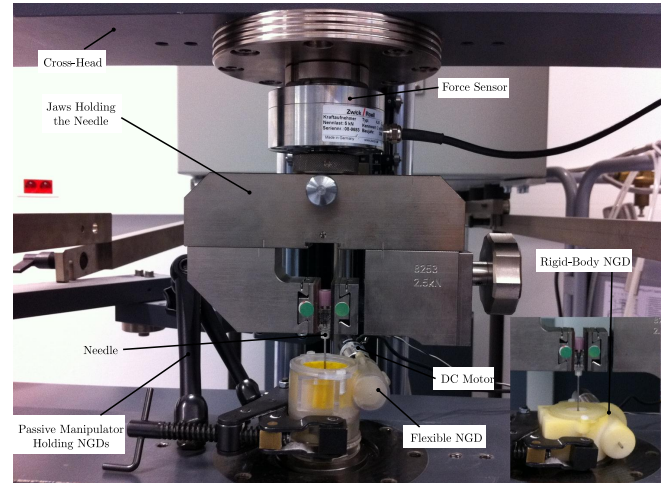


FIGURE 12. DESCRIPTION OF EXPERIMENTAL SETUP.

In Figure 12, essential components of the experimental setup namely the cross-head, force sensor, needle, two NGDs and a passive manipulator for holding the NGDs rigidly during experiment can be seen. Force is applied to the cross-head by the traction machine, which in turn applies the force on the needle grasped tightly between the NGD. During the experiments there is no slipping between the proximal end of the needle and the chuck jaws of the traction machine, so NGD experiences the same amount of force. Input current to the motor was maintained constant, so as to maintain constant grasping force for each experiment. Also length of the needle, at which the NGDs grasp it, is same for all experiments. This was done to have the same constant set of conditions at the beginning of each experiment.

4.2 Results

In this section, some results of the traction experiments conducted on the proposed NGDs and a qualitative and quantitative comparison of their respective performances, are presented. A total of the 58 experiments were conducted

on the rigid-body NGD and total of the 46 experiments on the flexible NGD. For the rigid-body NGD experiments were stopped after slipping of 4 mm, whereas for flexible NGD experiments were stopped after slipping of 6 mm, as can be seen in Figure 13(b).

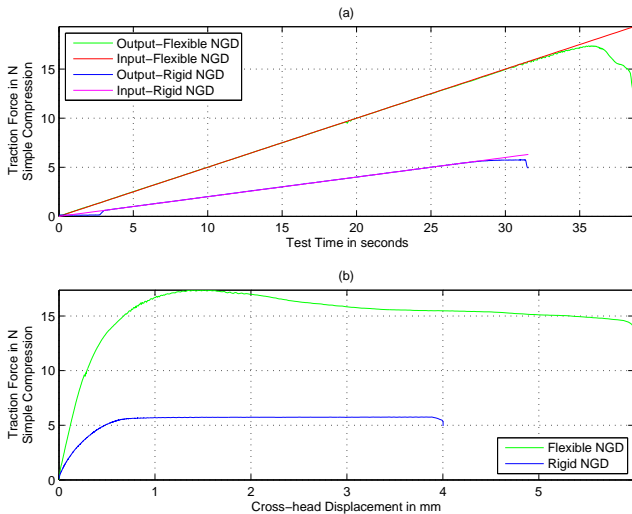


FIGURE 13. RESULTS OF THE SIMPLE COMPRESSION LOADING.

During needle insertion one can observe two distinctive phases in force profile i) a phase of constant rate of change of force when needle is being inserted gradually through tissue of uniform density ii) a phase where force suddenly decreases over very small periods of time, for example during tissue ruptures or sudden changes in tissue density. Therefore, these experiments were designed in two parts: i) In first part, input rate of change of force was kept constant, which is called here simple compression loading. ii) In second part, different segments in input force profile each segment with a varying rate of change of force, which is called here the variable loading, were introduced.

For first part of the experiments rate of change of force was kept constant, as in Figure 13. Typical results for simple compression loading for Rigid-NGD and for Flexible-NGD are presented. In Figure 13(a), it can be seen that both NGDs are capable to comply with input force, as curves for input and output fall on each other, until a certain threshold force, when the slipping occurs. Also it can be observed, that value of the threshold force for flexible NGD is much higher than that for rigid body NGD.

For the second part of the experiments, force was allowed to drop suddenly, hence creating a rate of change of force of order 1kN/s, magnitude of which agrees with data

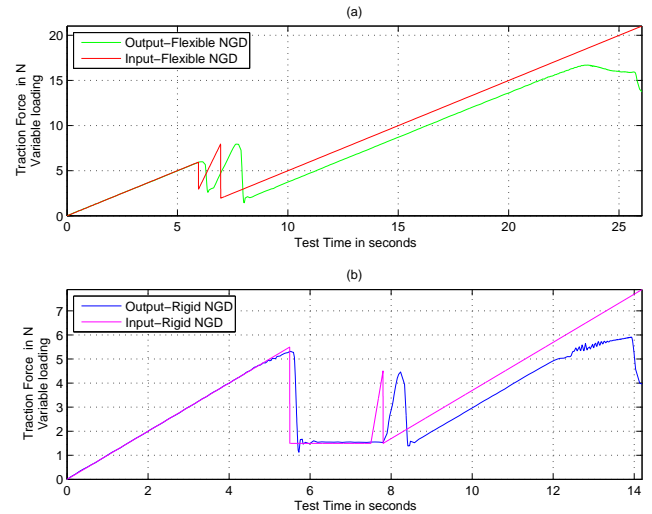


FIGURE 14. RESULTS OF THE VARIABLE LOADING.

from *in vivo* experimental data presented in [1].

In Figure 14(a) and 14(b), two such instances of sudden drop in forces were allowed. It can be seen that before this sudden change compliance of the NGDs with input force profile is very good. At the first drop, It was observed that there is a short time delay between the input and output. There is rough compliance with upper and lower levels of the force but time taken is evidently larger. This effect is more pronounced after second drop of the force and It can be clearly seen, that there is some time delay between the input force and output traction force, but again there is rough compliance with upper and lower levels of force. For the flexible NGD and the curve shown in Figure 14(a) average of absolute difference for the upper and lower levels of force is less than 0.02 N and 0.5 N respectively. For the rigid NGD and the curve shown in Figure 14(b) average of absolute difference for the upper and lower levels of force is less than 0.1 N and 0.2 N respectively. Therefore, both NGDs are capable of reproducing sudden change in input force, without letting the needle slip though with a time delay importance of which grows with number of such sudden changes in force. In a way, this points to a limit of rate of change of force to which NGDs can comply with. Experiments are allowed to continue after the sudden changes in input force to test for threshold force at which slipping occurs.

During needle insertion stiffness plays an important role, for needle must not slip when there are sudden and large changes in the force. Stiffness here is defined as slope of the straight line passing from the point on curve in the Figure 13(b) through the origin. In Figure 15(a) and Figure 15(b), the quantitative measures of the stiffness at dif-

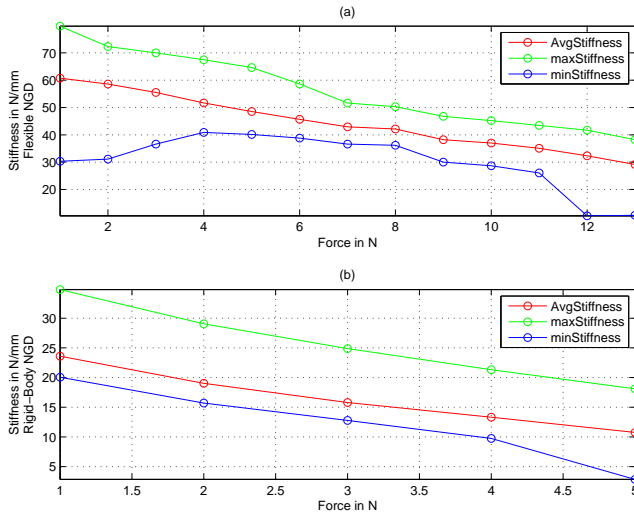


FIGURE 15. STIFFNESS CHARACTERISTICS OF THE NGDs.

ferent levels of the input force are presented. This figure also describes the average value of slipping for both NGDs at different force levels, which can be obtained by dividing the force level with average stiffness value. Threshold value of force at which needle starts slipping is not very well defined and ideally it should be defined as the force at which instantaneous slope of the curve shown in Figure 13(b) is nearing to zero. Here threshold value has been defined as force at which needle has slipped by 0.5 mm. This definition is more conservative than ideal one and required for safety considerations. Magnitude of this threshold value is less than ideal threshold value. In Figure 15 limit of the 13 N for flexible NGD and limit of the 5 N for rigid-body NGD were chosen, because at these force limits respective NGDs have slipped on an average of less than 0.5 mm. As evident from this figure average stiffness of the sample decreases as force increases.

A comparative study of the above figures suggests, that flexible NGD outperforms the rigid-body NGD both in the value of threshold force and stiffness values. This is of course influenced by several factors which might be improved by, for example, using a material of higher coefficient of friction between the NGD and the needle to improve the traction force.

5 CONCLUSION

The availability of NGD appears to be a limiting factor to the development of robotized needle insertion assistants. In this paper, the current development of our latest NGD based on flexible parts were presented. The first compara-

tive experimental assessments of this new embodiment reveal a much higher performance level than the previously developed NGD based on rigid bodies. The flexible NGD has a wider aperture to allow free motion of the needle when it is required by the medical procedure but remains compatible with needle regrasping. The measured traction force transmitted to the needle is also improved by a three times higher factor. Future work includes additional tests to assess the flexible NGD behavior using other standard needle sizes and the integration of the proposed NGD into one novel needle insertion assistant.

REFERENCES

- [1] Piccin, O., Barbé, L., Bayle, B., de Mathelin, M., and Gangi, A., 2009. "Force feedback teleoperated needle insertion device for percutaneous procedures". *International Journal of Robotics Research*, **28**(9), Sept., pp. 1154–1168. Special issue on Medical Robotics.
- [2] Stoianovici, D., Cleary, K., Patriciu, A., Mazilu, D., Stanimir, A., Craciunoiu, N., Watson, V., and Kavoussi, L., 2003. "Acubot: a robot for radiological interventions". *Robotics and Automation, IEEE Transactions on*, **19**(5), oct., pp. 927 – 930.
- [3] Walsh, C. J., Hanumara, N. C., Slocum, A. H., Shepard, J.-A., and Gupta, R., 2008. "A patient-mounted, telerobotic tool for CT-guided percutaneous interventions". *Journal of Medical Devices*, **2**(1), p. 011007.
- [4] Badaan, S., Petrisor, D., Kim, C., Mozer, P., Mazilu, D., Gruionu, L., Patriciu, A., Cleary, K., and Stoianovici, D., 2011. "Does needle rotation improve lesion targeting?". *The International Journal of Medical Robotics and Computer Assisted Surgery*, **7**(2), pp. 138–147.
- [5] Piccin, O., Renaud, P., Barbé, L., Bayle, B., Maurin, B., and de Mathelin, M., 2005. "A robotized needle insertion device for percutaneous procedures". In *Proceedings of the 2005 ASME Design Engineering Technical Conferences*, pp. 433–440.
- [6] Pahl, G., Beitz, W., Feldhusen, J., and Grote, K.-H., 2007. *Engineering Design – A Systematic Approach*. Springer.
- [7] Howell, L. L., 2001. *Compliant Mechanisms*. John Wiley & Sons, Inc, New York.
- [8] Trantina, G., and Nimmer, R., 1994. *Structural analysis of thermoplastic components*. McGraw-Hill.